Low-symmetry phases at the tilt boundary of the $Pb(Zr_{1-x}Ti_x)O_3$ solid solution

Guillaume Fraysse,[1,*] Julien Haines,[1] Véronique Bornand,[1] Jérôme Rouquette,[1] Marie Pintard,[1] Philippe Papet,[1] and Steve Hull[2]

[1]*Institut Charles Gerhardt Montpellier, UMR 5253 CNRS-UM2-ENSCM-UM1, Physico-chimie des Matériaux Organisés Fonctionnels, Université Montpellier II, Place Eugène Bataillon, 1504, 34095 Montpellier Cedex 5, France*

[2]*ISIS Science Division, Rutherford Appleton Laboratory, Chilton, Didcot, Oxfordshire OX11 0QX, United Kingdom*

(Received 4 July 2007; revised manuscript received 22 December 2007; published 19 February 2008)

The tilt boundary that separates the well-known rhombohedral phases *R*3*m* and *R*3*c* of the $Pb(Zr_{1-x}Ti_x)O_3$ solid solution was investigated by means of time-of-flight neutron powder diffraction, dielectric measurements, and resonance Raman spectroscopy. Careful Rietveld refinements yield significantly better agreement factors using monoclinic models for the long-range structure of $PbZr_{0.6}Ti_{0.4}O_3$ with a *Cc* space group at low temperature and with a *Cm* space group at high temperature rather than the widely accepted rhombohedral symmetry. The spontaneous polarization was found to lie along the pseudocubic [112] direction instead of along the [111] direction. This polarization direction is shown to be adopted for a wide variety of compositions, temperatures, and pressures and has major implications for the domain structure of these materials. Furthermore, the transition between the untilted and the tilted structures was found to be very diffuse and strongly dependent on the thermal history of the sample.

DOI: 10.1103/PhysRevB.77.064109 PACS number(s): 77.84.Dy, 61.50.Ks, 61.05.fm, 77.80.Bh

I. INTRODUCTION

The lead zirconate titanate $Pb(Zr_{1-x}Ti_x)O_3$ solid solution (PZT) has been the subject of a considerable number of studies not only because of its technological importance for piezoelectric transducer and actuator applications but also for its fundamental aspects. This perovskite solid solution is characterized by a rich and complex phase diagram. At high temperatures, these compounds exhibit a high symmetry primitive cubic perovskite structure. At lower temperatures, a variety of cation shifts, octahedral tilts, and distortions occur leading to a number of different structures: the antiferroelectric orthorhombic *Pbam* structure of $PbZrO_3$. With increasing Ti content, two ferroelectric rhombohedral phases are observed up to the morphotropic phase boundary (MPB) (x_{Ti}=47%). The low-temperature *R*3*c* phase differs from the high temperature *R*3*m* phase in that the oxygen octahedra are tilted about the $[111]_{pc}$ direction resulting in the doubling of the unit cell. The boundary between these rhombohedral phases, known as the tilt boundary, is associated with a high pyroelectric figure of merit and has been established by Jaffe *et al.*[1] for temperatures higher than 300 K and extended to low temperature by Amin *et al.*[2] for x=40% and more recently by Noheda *et al.*[3] for x=42%. For compositions between the MPB and the end member $PbTiO_3$, there is a ferroelectric tetragonal *P*4*mm* phase. This information represents the accepted view of the PZT phase diagram that persisted until a few years when new data began to emerge, providing new evidence of low-symmetry phases.

The high piezoelectric coupling constants observed for "morphotropic compositions" have long been attributed to the simultaneous presence of rhombohedral and tetragonal domains until it has been demonstrated that the maximum electromechanical response was obtained for compositions outside what has been supposed to be a region of two-phase coexistence.[4] The discovery of a monoclinic ferroelectric phase in this narrow region of the phase diagram proved to be a breakthrough in understanding such MPB systems.[5] This monoclinic phase F_M with space group *Cm* serves as a transition bridge between the higher symmetry F_T and F_R phases. In this phase, the direction of polarization can lie anywhere between the pseudocubic [001] and [111] directions, thus providing a possible explanation for this high piezoelectric response.[6,7]

Additionally, a second monoclinic phase with a doubled unit cell has been observed at low temperatures for $PbZr_{0.52}Ti_{0.48}O_3$.[8] This second monoclinic phase has been the subject of many controversies such as its exact space group, the axis about which the oxygen octahedra tilt, and even if it is a minority phase rather than the long-range ground state.[9–14] Theoretical calculations[15] confirm the finding of Hatch *et al.*[10] that the space group for the low temperature phase is *Cc* rather than *Pc*. Furthermore, the *Cc* phase is found to be the long-range-ordered ground state rather than a minority phase coexisting with the *Cm* phase. These results are also in agreement with those obtained by electron diffraction,[16] which show that the oxygen octahedra in the *Cc* phase rotate about an axis that is between the [001] and [111] directions.

Other low-symmetry phases have been discovered close to the antiferroelectric-ferroelectric phase boundary, which separates the *Pbam* antiferroelectric phase from the well-known rhombohedral *R*3*m* and *R*3*c* phases. By analogy with a study on La-doped PZT,[17] it was proposed that the new untilted structure has *Pm* symmetry and that the introduction of the $a^-b^-b^-$ tilt system results in *Pc* symmetry. Moreover, it was proposed that the tilt boundary separating tilted and untilted structures crosses the MPB. This yields a phase with *Cc* symmetry, a result of combining the ionic displacements of the *Cm* cell with the $a^-b^-b^-$ tilt system. Further extension of this tilt boundary can be made due to the discovery of a low temperature tetragonal phase with *I*4*cm* space group, which also involves a coexistence of ferroelectricity and tilting of oxygen octahedra.[15] This tilting occurs at low temperature, resulting in the transformation of the four untilted

 ©2008 The American Physical Society

ferroelectric *Pm*, *R*3*m*, *Cm*, and *P*4*mm* phases to four additional ferroelectric phases with *Pc*, *R*3*c*, *Cc*, and *I*4*cm* space groups, respectively. Understanding the nature of this tilt boundary is, therefore, of great importance.

Although the structure of zirconium-rich compositions of PZT is widely accepted to be rhombohedral for compositions lying between the antiferroelectric-ferroelectric and the morphotropic phase boundaries, some recent studies indicate that the true symmetry may be lower. Anomalous anisotropic displacement parameters of the cations were obtained in a neutron diffraction investigation of a series of "rhombohedral" compositions.[18] In order to reconcile these observations, the authors have proposed a model in which Pb cations are shifted not only along the $[111]_p$ direction as the other atoms but also randomly along the three $\langle 100\rangle_p$ directions. The resulting average structure is still rhombohedral but is monoclinic at the local unit cell level, with the same space group *Cm* as the monoclinic phase discovered for morphotropic compositions. Glazer *et al.*[19] have proposed that upon approaching the morphotropic phase boundary, the locally ordered regions present for pseudorhombohedral compositions grow until they form monoclinic regions large enough to scatter coherently and then decrease for tetragonal Ti-rich compositions. The morphotropic phase boundary is no longer considered by Glazer *et al.*[19] as a transition between the rhombohedral and the monoclinic phases. They suggest that it is the growth and then the disappearance of long-range order with increasing titanium content which could be responsible for the high piezoelectric and electromechanical coupling factors rather than the well-known polarization rotation mechanism.[6,7] Another argument in favor of a lower symmetry description came from x-ray diffraction studies[20] for $0.2<x<0.47$, in which anomalous broadening of the pseudocubic 200 reflection with respect to the pseudocubic 111 reflection was observed. This observation implies that the pseudocubic 200 reflection is split. Since it is unsplit in rhombohedral *R*3*m* and *R*3*c* symmetries, it was proposed that the structure is not rhombohedral for $0.38<x<0.47$ but is most likely monoclinic. A phase diagram was thus proposed in which the monoclinic phase exhibits an extended stability range.[21] Based on the previously reported splitting of the 200_{pc} reflection at low temperature,[20] the rhombohedral low temperature phase should be also monoclinic. Following the discoveries of a triclinic phase of La-modified $Pb(Zr_{0.65}Ti_{0.35})O_3$ at 40 K (Ref. 22) and the monoclinic *Pm* and *Pc* phases of PZT near the antiferroelectric-ferroelectric phase boundary,[16] a reconsideration of the stability field of the rhombohedral phases is necessary.

II. EXPERIMENT

$PbZr_{0.6}Ti_{0.4}O_3$ was prepared by the conventional solid-state reaction from high-purity (>99.9%) oxides via a two-stage calcination process.[23] Inductively coupled plasma analysis of the resulting powder sample gives the following Pb:Zr:Ti compositional range: 1.000(5):0.593(5):0.407(5). Time-of-flight neutron powder diffraction data were obtained as a function of temperature at the ISIS spallation source of the Rutherford Appleton Laboratory, on the Polaris medium resolution diffractometer as described previously,[24] and on the General Materials (GEM) diffractometer. Low temperature diffraction data were obtained using an orange cryostat. Temperatures were typically found to vary less than 1 °C during acquisition time. Structural refinements were performed with the Rietveld refinement program GSAS[25] on data collected with detectors in backscattering geometry ($130° < 2\theta < 160°$), due to their higher resolution. In the refinements, the cell parameters, atomic positions, atomic displacement parameters, scale factor, background, and line shape parameters were varied. Anisotropic atomic displacement parameters were refined only for the lead and oxygen atoms of PZT. Symmetry- and *hkl*-dependent anisotropic microstrain parameters (S_{hkl}) as implemented in GSAS line shape 4 were also included.[26] In recent studies, this line shape function was found to be particularly well suited to model the microstrain present in PZT ceramics.[27,28] It should be noted that the reflections were relatively broad due to microstrain broadening and compositional fluctuation which are always present in PZT ceramics and, therefore, that the resolution of the diffractometer was not a limiting factor. A monoclinic $P2_1/c$ ZrO_2 phase was included in the Rietveld refinement to take into account some very low-intensity peaks which do not correspond to the PZT structure. Weight fraction of this phase was found to be always less than 1%. Dielectric measurements were carried out on disk-shaped pellets with platinum electrodes sputtered on both sides. The dielectric susceptibility ε_r' and losses tan δ were studied as a function of heating and cooling in the temperature range of 190–370 K at the rate of 1 K min^{-1} with a Novocontrol BDS 4000 dielectric spectrometer. Raman experiments were performed as a function of temperature (10–350 K) using an Oxford Instrument Microstat closed-cycle helium cryostat. Resonance Raman spectra were obtained with an argon-krypton laser (647.1 nm) and a Jobin-Yvon T64000 triple monochromator equipped with an Olympus microscope and a charge-coupled device cooled down to 140 K. The temperature was measured near the sample using a silicon diode.[29,30] All figures in the parentheses refer to estimated standard deviations.

III. RESULTS AND DISCUSSION

A. Room-temperature structure of $PbZr_{0.6}Ti_{0.4}O_3$

Neutron data for $PbZr_{0.6}Ti_{0.4}O_3$ were first refined, at room temperature, with the *R*3*m* space group as in previous studies, and good agreement for the resulting cell parameters with previously published values[2] was obtained. Refinement of the structure using the *R*3*m* space group accounts for many of the features of the neutron powder diffraction profile; however, an unsatisfactory fit between the observed and the calculated profile and rather poor agreement factors are obtained, even when using S_{hkl} microstrain parameters and anisotropic displacement parameters for all the atoms (Fig. 1). Corker *et al.*[18] have already reported structure refinements using powder diffraction data, in which reasonable profile fits are obtained using rhombohedral symmetry only if unreasonable anisotropic displacement parameters are al-

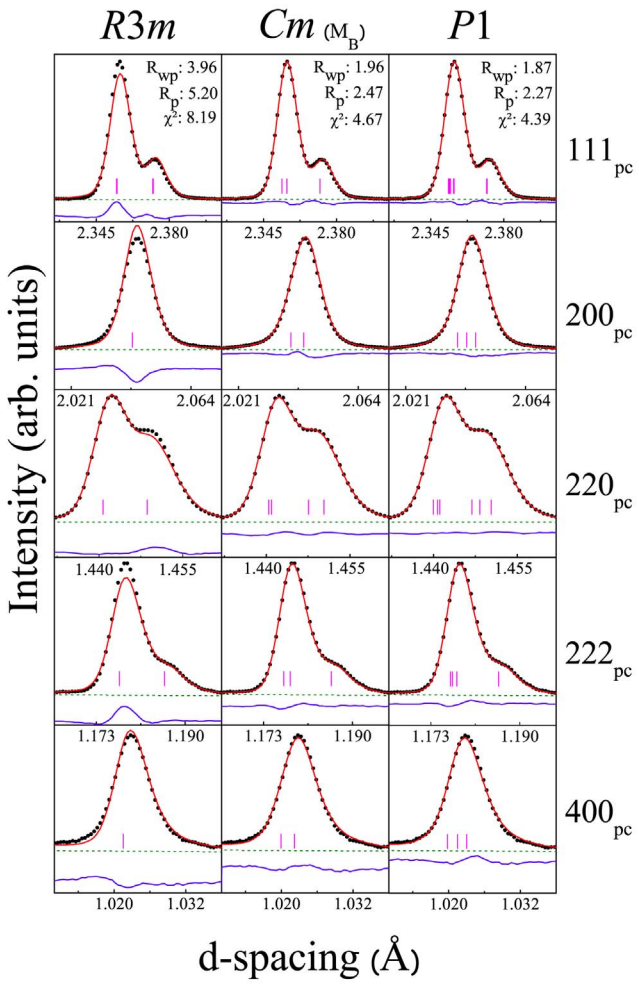

FIG. 1. (Color online) Observed (dots), calculated (continuous line), and difference (bottom line) neutron powder diffraction profiles of some selected pseudocubic reflections obtained from the Rietveld refinement of $PbZr_{0.6}Ti_{0.4}O_3$ at 294 K using the $R3m$ space group, Cm space group, and $P1$ space group. Vertical ticks indicate the calculated positions of the Bragg reflections. Overall agreement factors obtained for each structural model are also given.

lowed. In order to reconcile with these observations, a model was proposed in which the Pb atoms randomly occupy three disordered sites shifted along the pseudocubic ⟨100⟩ directions with respect to a common [111] direction. Therefore, the following models of locally disordered rhombohedral structures were tested: in the first, Pb atoms occupy the $(x,2x,z)$ position instead of the $(0,0,z)$ position, in the second, the (x,y,z) position, and in the third, Pb, Zr, and Ti atoms occupy three $9b(x,2x,z)$ positions. None of these models markedly improved the fit between the observed and calculated profiles. These models were not considered any further. The asymmetry of the profile that one can observe on the lower d-spacing side of the 200 and 400 pseudocubic reflections and on the higher d-spacing side of the 220 pseudocubic reflection can definitively not be explained using a rhombohedral structure. Such anomalous peak broadening has already been observed for zirconium-rich compositions of PZT[20] and for La-modified $PbZr_{0.65}Ti_{0.35}O_3$ (Ref. 22) and has been considered as evidence for a monoclinic or a triclinic structure, with a Cm or $F1$ space group, respectively. The monoclinic Cm group was considered in our refinements for $PbZr_{0.6}Ti_{0.4}O_3$. As can be seen in Fig. 1, this leads to the significant improvement in the fit between the observed and calculated profiles and considerably lower agreement factors. A similar improvement in the fit using a monoclinic Cm model in combination with anisotropic peak broadening parameters instead of rhombohedral $R3m$ symmetry has been recently reported in a high resolution synchrotron x-ray diffraction study[31] of $PbZr_{0.575}Ti_{0.425}O_3$. Since triclinic phases have been discovered for 7% La-modified $PbZr_{0.65}Ti_{0.35}O_3$ (PLZT) at 40 K,[22] where a rhombohedral symmetry was expected, and for titanium-rich compositions of PZT at high pressure,[24] a triclinic $P1$ model was also considered. The resulting agreement factors are slightly lower than those obtained using a monoclinic Cm model.

No superlattice reflections were observed in the profile. Nevertheless, as the F_{LT}-F_{HT} phase transition is of first order, the composition $PbZr_{0.6}Ti_{0.4}O_3$ lies in a region of two-phase coexistence at 294 K. Thus, two-phase models were also considered in our refinements. The $R3m+R3c$ model gave better agreement factors ($R_{wp}=3.15$, $R_p=4.44$, $\chi^2=5.346$) than those obtained using a single rhombohedral phase, but still high in comparison with monoclinic and triclinic single-phase models ($R_{wp}=1.96$, $R_p=2.47$, $\chi^2=4.67$ and $R_{wp}=1.87$, $R_p=2.27$, $\chi^2=4.39$, respectively). Furthermore, the calculated positions of the Bragg reflections reveal that, during the refinement, the $R3c$ phase only took into account the intensity mismatch at the base of the Bragg peaks.

Cell parameters, fractional atomic coordinates, and atomic displacement parameters obtained for the Cm model at 294 K are given in Table I. The small U_{iso} of the Zr and Ti atoms with respect to the U_{eq} of the Pb and O atoms might be due to size difference between Zr and Ti.[22]

B. Structure of $PbZr_{0.6}Ti_{0.4}O_3$ at 1.5 K

Superlattice reflections present in the neutron powder diffraction profile of $PbZr_{0.6}Ti_{0.4}O_3$ at 1.5 K are consistent with a structure with a doubled unit cell resulting from tilts of the oxygen octahedra. These all-odd hkl reflections (311, 313, 333, 511,…) with respect to a doubled elementary perovskite unit cell arise due to antiphase (−) tilts of the neighboring $(Zr,Ti)O_6$, as was shown by Glazer.[32,33] It should be noted that the most prominent reflection (i.e., the pseudocubic $\frac{3}{2}\frac{1}{2}\frac{1}{2}$ reflection, shown in Fig. 2) has only 3% relative intensity with regard to the pseudocubic 111 reflection. Since these superlattice reflections are essentially due to oxygen displacements, they can be expected to be extremely weak in x-ray diffraction because of the low relative x-ray scattering factor of oxygen. The use of neutron diffraction is, therefore, necessary to determine the fine structure of this low temperature form.

Since the low temperature structure of $PbZr_{0.6}Ti_{0.4}O_3$ is widely accepted to be rhombohedral, neutron data were first refined with $R3c$ space group. For this space group, the ionic displacements along the pseudocubic [111] direction of the $R3m$ cell are combined with the $a^-a^-a^-$ tilt system. Rietveld

TABLE I. Structural data (cell parameters, fractional atomic coordinates, and isotropic—for Zr, Ti—or equivalent atomic displacement parameters) and agreement factors for monoclinic *Cm* and *Cc* models of $PbZr_{0.6}Ti_{0.4}O_3$ at 294 and 1.5 K, respectively. *Cm*: origin at Pb position. Site Pb, Zr/Ti, O(1) $2a(x,0,z)$, O(2) $4b(x,y,z)$. *Cc*: origin based on Pb x and z coordinates $(0,y,0)$. Site $4a(x,y,z)$.

	T=294 K, *Cm* space group (M_B type) R_{wp}=1.96, R_p=2.47, χ^2=4.67 a=5.8016(1) Å, b=5.7637(1) Å, c=4.0798(1) Å, β=90.403(1)°, V=136.421(2) Å^3				T=1.5 K, *Cc* space group (M_B type) R_{wp}=2.13, R_p=3.46, χ^2=0.76 a=9.9587(2) Å, b=5.7553(1) Å, c=5.7987(1) Å, β=125.100(1)°, V=271.915(7) Å^3			
Atom	x	y	z	100*U	x	y	z	100*U
Pb	0	0	0	2.47(2)	0	0.7526(5)	0	0.83(1)
Zr,Ti	0.4587(1)	0	0.5333(4)	0.41(1)	0.2314(4)	0.2527(13)	0.1862(15)	−0.01(1)
O(1)	0.4246(2)	0	0.0381(5)	1.55(3)	−0.0234(2)	0.2752(2)	−0.1057(2)	0.64(2)
O(2)	0.1854(1)	0.2428(1)	0.5463(3)	1.60(1)	0.2307(1)	0.4877(3)	−0.0988(2)	0.77(2)
O(3)					0.2109(1)	−0.0040(3)	0.4005(3)	0.74(2)

refinements using this rhombohedral model lead to rather poor agreement factors (R_{wp}=3.6, R_p=5.01, χ^2=1.27) and unsatisfactory fit between the observed and the calculated profiles (Fig. 2). As in the case of the room-temperature data, anomalous peak broadening is observed, indicating that the symmetry is lower than rhombohedral. Therefore, lower symmetries were considered in our refinements. According to Glazer's classification,[32] two antiphase tilt systems correspond to lower symmetries, namely, $a^-b^-b^-$ and $a^-b^-c^-$ tilt systems. Therefore, *Cc* and *F*1 space groups may be considered for the refinement as they result from the loss of the inversion center of the $C2/c$ and *F*1 space groups, associated with these tilt systems. A significant improvement in the fit between the observed and calculated profiles and low agreement factors (R_{wp}=2.13, R_p=3.46, χ^2=0.76) were obtained using a *Cc* model. Refinements using *F*1 space group (standard setting *P*1 with added face-centred generators) lead to slightly lower agreement factors (R_{wp}=1.92, R_p=3.2, χ^2=0.68) than those obtained using a monoclinic *Cc* model and, above all, a much better fit to the superlattice reflections. Structural data obtained for the *Cc* model at 1.5 K are given in Table I.

C. Ferroelectric F_{LT}-ferroelectric F_{HT} phase transition in $PbZr_{0.6}Ti_{0.4}O_3$

In order to follow the phase transition between the low and the high temperature ferroelectric phases of $PbZr_{0.6}Ti_{0.4}O_3$, the crystal structure was refined at 25 further temperatures. Two sets of measurements were performed at a few month interval on the Polaris diffractometer. The sample was first placed in the cryostat and quickly cooled down to 4 K. The first set was performed on heating, starting from 100 K. For the second set, measurements were performed on the same sample but on slow cooling starting from room temperature to 1.5 K and then on heating to 270 K. Thus, at the beginning of the two sets of measurements, the sample is characterized by a different thermal history. It should be noted that Rietveld refinements of the neutron data using this monoclinic model always lead to considerably lower agree-

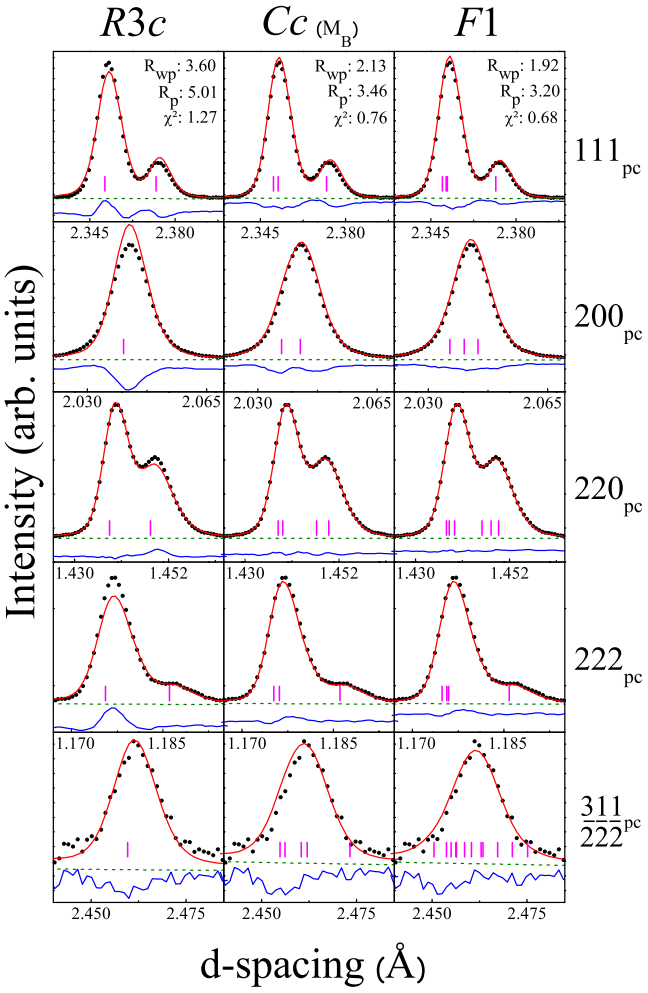

FIG. 2. (Color online) Observed (dots), calculated (continuous line), and difference (bottom line) neutron powder diffraction profiles of some selected pseudocubic reflections obtained from the Rietveld refinement of $PbZr_{0.6}Ti_{0.4}O_3$ at 1.5 K using the $R3c$ space group, *Cc* space group, and *F*1 space group. Vertical ticks indicate the calculated positions of the Bragg reflections. Overall agreement factors obtained for each structural model are also given.

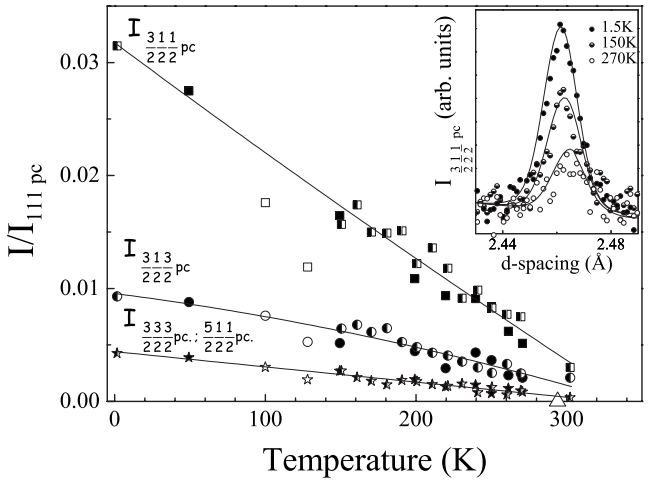

FIG. 3. Temperature dependence of the integrated intensity of the most prominent superlattice reflections observed for $PbZr_{0.6}Ti_{0.4}O_3$. Intensities are normalized with respect to the pseudocubic 111 reflection. Open symbols correspond to the first set of measurements (rapid cooling), and half-solid and solid symbols to the second set (slow cooling), on decreasing and increasing temperature, respectively. Inset illustrates the evolution of the pseudocubic $\frac{3}{2}\frac{1}{2}\frac{1}{2}$ superlattice reflection as a function of temperature.

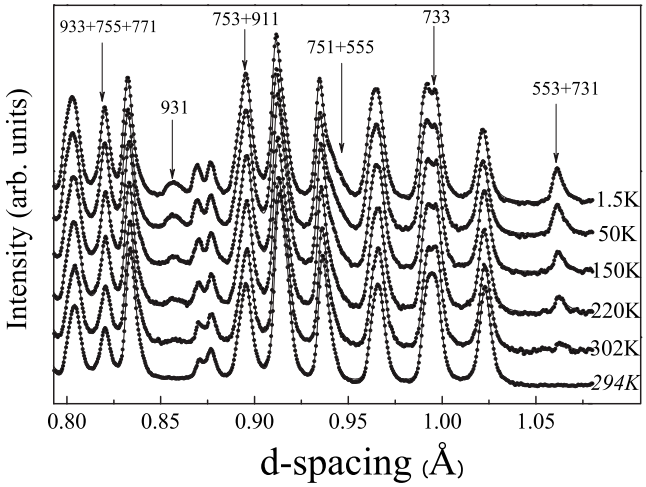

FIG. 4. Influence of the superlattice reflections on a selected *d*-spacing range of the observed and calculated neutron powder diffraction profiles of $PbZr_{0.6}Ti_{0.4}O_3$ as a function of temperature. Arrows indicate the position of the superlattice reflections (indexed on a $2a \times 2a \times 2a$ pseudocubic unit cell). The room-temperature profiles of the first set of measurements are also added (in italics).

ment factors than those obtained with the widely accepted rhombohedral models.

1. Superlattice reflections, cell parameters, and relative volume as a function of temperature

The temperature dependence of the integrated intensity of the most prominent superlattice reflections is shown in Fig. 3. It is obvious that the first set of measurements (open symbols) shows significant differences with respect to the second set (half-solid and solid symbols). Integrated intensities of the superlattice reflections obtained for the first set at 128 K are clearly lower than those extrapolated from the second set. A more striking difference should be noted at room temperature. Whereas no superlattice reflections are observed at 294 K for the first set, indicating that the structure is untilted, superlattice reflections are still present for the second set, even at higher temperature (302 K). Thus, if the second set data are considered, the phase transition should occur beyond 302 K, while it should occur about 100 °C lower considering the first set. This fact may be explained by the existence of a broad region of two-phase coexistence. The F_{LT}-F_{HT} phase transition is thus of a very diffuse type and the transition temperature is strongly dependent on the thermal history of the sample.

The strong dependence of the structure on the sample's thermal history is clearly noticeable in the 0.8–1.1 Å *d* spacing range. In Fig. 4, observed and calculated profiles of some selected temperatures of the second set are shown for this *d*-spacing range. The room-temperature profiles of the first set are also added. The 931 and the 553+731 superlattice reflections (indexed on a $2a \times 2a \times 2a$ pseudocubic unit cell) are still observable in the neutron profile at 302 K (second set), while they have already disappeared at 294 K for the first set. Moreover, evidence of a gradual decrease in intensity of these superlattice reflections with increasing temperature is shown. This can clearly be seen even when the superlattice reflections are merged with ordinary reflections. The peak at 0.82 Å is found to decrease with respect to surrounding peaks as a result of the disappearance of the 933, 755, and 771 superlattice reflections. In the same way, one can easily observe the disappearance of both the splitting of the peak at 0.99 Å and the shoulder on the higher *d*-spacing side of the peak at 0.94 Å.

The assumption of a large region of two-phase coexistence is confirmed by the evolution of the cell parameters and the relative volume as a function of temperature, shown in Fig. 5 for the two sets of measurements. Considering the fit of the relative volume, it is clear that the values obtained at 100 and 128 K were overestimated with respect to those extrapolated from the second set. This may be explained by the fact that there is actually a certain amount of the untilted phase coexisting with the tilted phase and which is not taken into account during the Rietveld refinements (neutron data were refined using a single-phase model with doubled unit cell).

2. Dielectric measurements as a function of temperature

With increasing temperature, the dielectric susceptibility ε_r' and losses tan δ (see Fig. 6) both show a marked feature at 295 K, due to the ferroelectric F_{LT}-ferroelectric F_{HT} phase transition. This transition temperature is about 20 K higher than that recently reported by Eitel and Randall[34] based on low-field electromechanical resonance measurements and high-field unipolar strain measurements. As discussed previously, the thermal history of the sample may explain the difference in the transition temperature. On cooling, only a slight inflexion of the curves is observed. This hysteresis as a

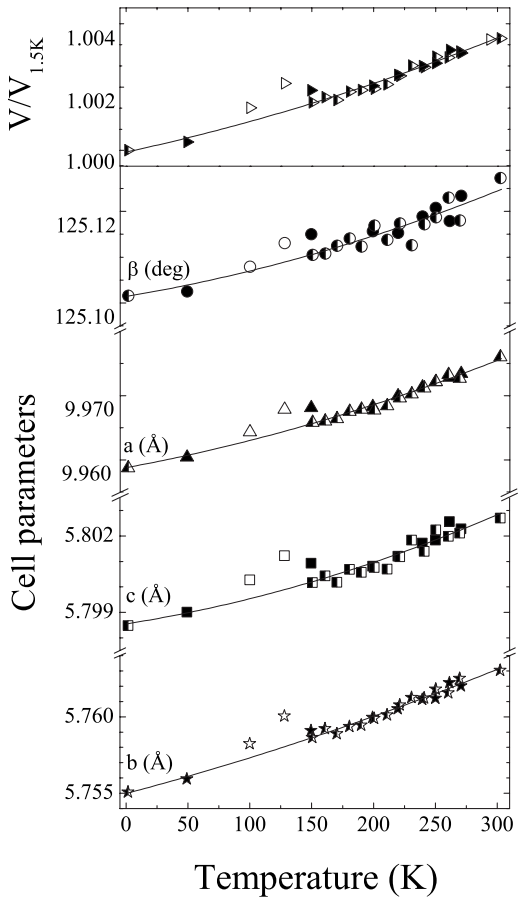

FIG. 5. Cell parameters and relative volume for the monoclinic *Cc* model as a function of temperature. Open symbols correspond to the first set of measurements (rapid cooling), and half-solid and solid symbols to the second set (slow cooling), on decreasing and increasing temperature, respectively.

function of heating and cooling is characteristic of a first-order phase transition.

3. Variable temperature study of $PbZr_{0.6}Ti_{0.4}O_3$ *using resonance Raman spectroscopy*

The phase transition between the low F_{LT} and the high F_{HT} temperature phase of $PbZr_{0.6}Ti_{0.4}O_3$ was also investigated by resonance Raman spectroscopy. A recent study has shown that this method is particularly useful in order to determine the phase transition sequence in ferroelectric systems such as PZT.[29] Raman spectra (10–725 cm^{-1}) were obtained, with increasing temperature, for a series of temperatures lying between 10 and 350 K (Fig. 7). Because of the lack of single crystals of PZT and the well-known static and dynamic disorder in this material, the assignment of each Raman mode is not possible. It should be noted that data obtained at 10 and 300 K are clearly different from previously reported spectra, recorded at 7 and 300 K on the same composition.[35,36] This is a result of the different excitation lines used to perform Raman experiments. Whereas Raman measurements generally reported in the literature on the PZT solid solution have been obtained using a 514.5 nm excitation line, Rouquette *et al.*[29] have shown that using an excitation line of 647.1 nm, which has an energy close to a self-trapped level exciton energy deficient complex (Ti_{Ti}'-$V_O^{\cdot\cdot}$) of PZT powder, induces a resonance phenomenon. This effect enables a clear dissociation of the different modes in the Raman spectra, at least at low temperatures, and thus makes the observation of structural changes easier.

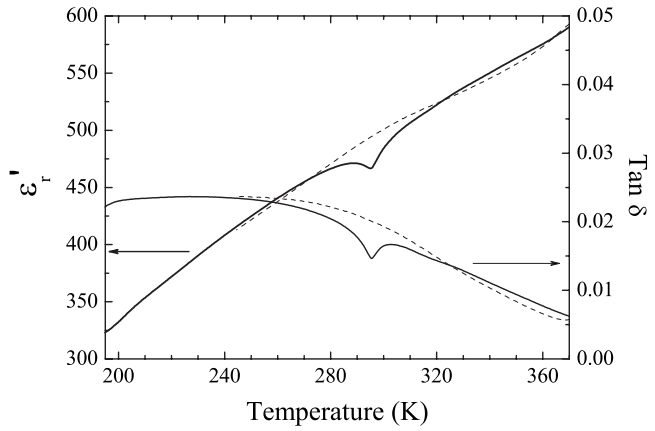

FIG. 6. Temperature dependence of the dielectric susceptibility (ε_r') and losses (tan δ) for $PbZr_{0.6}Ti_{0.4}O_3$ (solid line, increasing temperature; dashed line, decreasing temperature).

At 10 K, the Raman spectrum consists of three regions, 50–180, 180–400, and 400–725 cm^{-1}, each of which consists of many overlapped modes. With increasing temperature, an increase in the linewidths of the Raman modes oc-

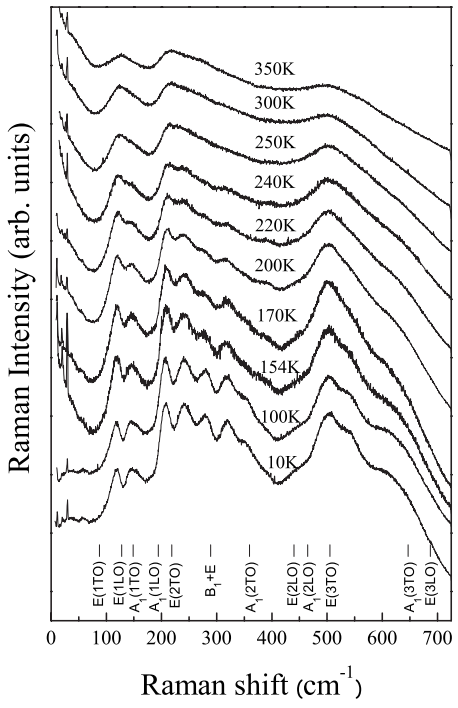

FIG. 7. Resonance Raman spectra of $PbZr_{0.6}Ti_{0.4}O_3$ obtained with the 647.1 nm excitation line as a function of temperature. Positions of the Raman peaks of $PbTiO_3$ at room temperature are indicated (see Ref. 48).

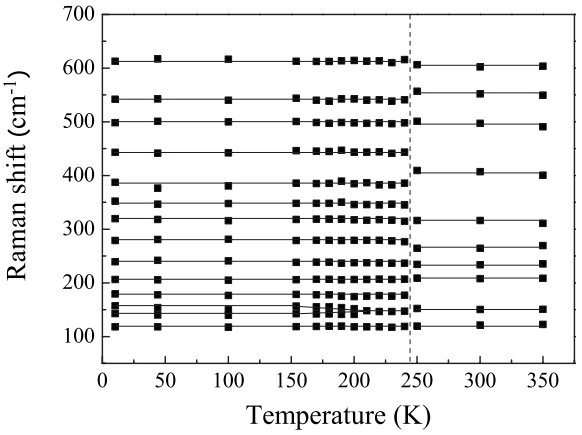

FIG. 8. Temperature dependence of the Raman modes. The temperature at which major spectral changes occur is indicated by a dashed line.

curs and the spectral lines shape become more symmetric starting from 250 K, indicating the disappearance of several modes and thus the transition between the low and the high temperature phases. Group theory predicts 27 active modes for the monoclinic Cc model of $PbZr_{1-x}Ti_xO_3$ ($13A'+14A''$), as opposed to 11 active modes for the rhombohedral $R3c$ model ($4A_1+7E$). For the untilted structure, 12 active modes are predicted for the monoclinic Cm model ($7A'+5A''$), as opposed to 7 for the rhombohedral $R3m$ model ($3A_1+4E$). In order to obtain representative peak positions, the Raman spectra were deconvoluted by fitting the modes to Voigt functions. The disappearance of the modes at 180, 360, and 450 cm^{-1} is observed at a temperature higher than 240 K (Fig. 8), which have been reported for Ti-rich compositions to be linked to the doubled primitive unit cell.[30,37] Consequently, the phase transition appears to occur between 240 and 250 K. Nevertheless, the determination of a temperature transition using a deconvolution procedure has to be done with the utmost care. Indeed, for temperatures higher than 240 K, Raman spectra consist of three broad bands, each of which consists of several subpeaks. Therefore, it is difficult to observe the disappearance of one of these subpeaks and thus determine the exact temperature at which the phase transition occurs. Considering that the three broad bands are rather asymmetric at 250 and 300 K and become more symmetric from 350 K, notably the band located at about 125 cm^{-1}, the transition may equally well occur between 300 and 350 K.

Raman measurements confirm the findings of neutron powder diffraction and dielectric measurements that the phase transition between the low and the high temperature phases of $PbZr_{0.6}Ti_{0.4}O_3$ is very diffuse and thus the existence of a large region of two-phase coexistence.

D. Spontaneous polarization, polarization rotation, and octahedral tilting

The structural data can be used to calculate the spontaneous polarization P_S, as well as the polarization rotation with respect to the pseudocubic [001] direction [characterized by the rotation angles θ and φ (Ref. 24)]. If electronic polarization and domain contributions are neglected, the spontaneous polarization[11] can be estimated by the following dipole moment equation $\mathbf{P}_S \approx (1/V)\Sigma_i q_i \mathbf{r}_i$, where q_i and r_i are, respectively, the point charges (ions with their nominal charges) and their positions in the unit cell of volume V. Values of the spontaneous polarizations and the polarization rotation of the low and the high temperature ferroelectric phases of $PbZr_{0.6}Ti_{0.4}O_3$ are reported in Table II. A less marked decrease of P_S (Fig. 9), on increasing temperature, is observed for the second set of measurements (from 39.9 $\mu C/cm^2$ at 1.5 K to 36.5 $\mu C/cm^2$ at 302 K) than for the first set (35.3 $\mu C/cm^2$ at 294 K). As a discontinuous decrease of P_S may be expected at the first-order F_{HT}-F_{LT} phase transition, this is further evidenced that the transition between the untilted and the tilted phases is strongly dependent on the thermal history of the sample.

Whereas for rhombohedral PZT the spontaneous polarization is constrained by symmetry to be along the hexagonal c axis (corresponding to the $[111]_{pc}$ direction), for monoclinic Cm and Cc PZT, the spontaneous polarization can adopt any

TABLE II. Spontaneous polarization P_S, rotation angles (θ, φ), and octahedral tilt angles $(\omega_a, \omega_b, \omega_c)$ for monoclinic morphotropic PZT (in italics), monoclinic models of $PbZr_{0.6}Ti_{0.4}O_3$, triclinic PZT, and triclinic 7% La-modified $PbZr_{0.65}Ti_{0.35}O_3$ as a function of P and T.

	S.G.	T (K)	P (GPa)	P_S ($\mu C/cm^2$)	θ (deg)	φ (deg)	ω_a (deg)	ω_b (deg)	ω_c (deg)
$PbZr_{0.60}Ti_{0.40}O_3$	*Cm*	294	0.0001	35.3	70	0	0	0	0
$PbZr_{0.60}Ti_{0.40}O_3$	*Cc*	1.5	0.0001	39.9	65	0	2.6	2.6	1.6
$Pb_{0.93}La_{0.07}Zr_{0.65}Ti_{0.35}O_3$[a]	*F*1	40	0.0001	37.2	71.4	0.4	1.4	0.9	3.4
$PbZr_{0.52}Ti_{0.48}O_3$[b]	*F*1	295	4.9	21	71	12	1.5	1.8	2.7
$PbZr_{0.52}Ti_{0.48}O_3$[b]	*F*1	128	7.2	19	67	28	2.5	2.2	5.7
$PbZr_{0.40}Ti_{0.60}O_3$[c]	*F*1	295	9.6	8	76	24	3	3.1	4.3
$PbZr_{0.52}Ti_{0.48}O_3$[b]	*Cm*	*280*	*0.0001*	*37.6*	*19*	*0*	*0*	*0*	*0*
$PbZr_{0.52}Ti_{0.48}O_3$[b]	*Cc*	*47*	*0.0001*	*40.3*	*23*	*0*	*0.2*	*0.2*	*2.3*

[a]Reference 22.
[b]Reference 24.
[c]Reference 49.

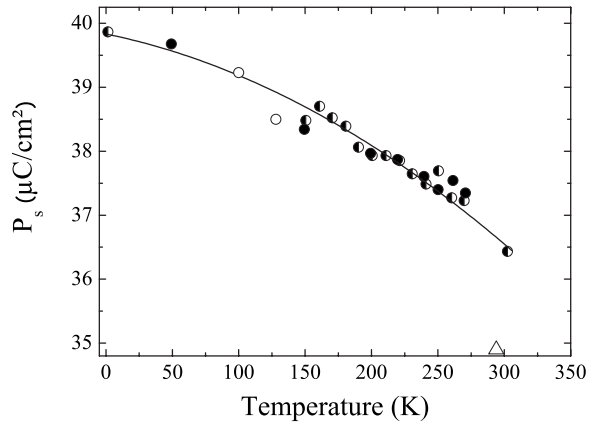

FIG. 9. Temperature dependence of the spontaneous polarization P_S for $PbZr_{0.6}Ti_{0.4}O_3$. Open symbols correspond to the first set of measurements, and half-solid and solid symbols to the second set, on decreasing and increasing temperature, respectively.

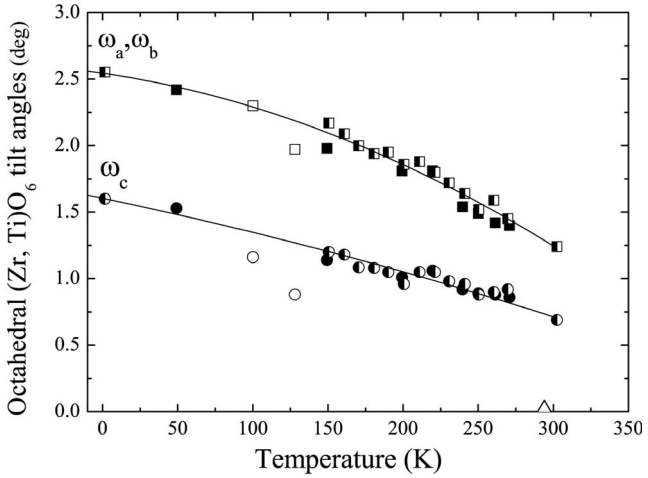

FIG. 10. Octahedral $(Zr,Ti)O_6$ tilt angles (deg) as a function of temperature for the monoclinic *Cc* model of $PbZr_{0.6}Ti_{0.4}O_3$. Open symbols correspond to the first set of measurements, and half-solid and solid symbols to the second set, on decreasing and increasing temperature, respectively.

orientation in the (110) plane. Thus, a rotation angle θ with respect to the pseudocubic [001] direction is necessary to describe this orientation. The use of the previously reported relationship[11] for monoclinic *Cm* and *Cc* models of $PbZr_{0.6}Ti_{0.4}O_3$ leads to θ angles of 70° and 65°, which are close to the pseudocubic [112] direction (θ=70.5°) and well beyond the 54.7° corresponding to rhombohedral symmetry. In recent studies, the polarization direction of triclinic 7% La-modified $PbZr_{0.65}Ti_{0.35}O_3$ at 40 K (Ref. 22) and of triclinic high-pressure forms of Ti-rich PZT solid solutions[24] was also found to lie close to this direction. Furthermore, according to Liu *et al.*, the complex domain structures observed for 7% La-modified $PbZr_{0.65}Ti_{0.35}O_3$ may be formed due to the change of polarization direction between the equivalent ⟨112⟩ directions.[22] As a low-symmetry model is consistent with the results at room temperature for pure PZT with a spontaneous polarization close to the $[112]_{pc}$ direction, the well-known non-180° domain of this phase may also be formed due to the change of polarization direction between the equivalent ⟨112⟩ directions. The present results show that the $[112]_{pc}$ polarization direction is adopted for a wide variety of compositions, temperatures, and pressures (see Table II) and has major implications for the domain structure of these materials.

It should be noted that these monoclinic models are pseudorhombohedral with $P_x=P_y>P_z$ and consequently are different from the monoclinic phases of M_A type ($P_x=P_y<P_z$) discovered near the morphotropic phase boundary.[5,8] The spontaneous polarization, rotation angles, and octahedral tilt angles of the $PbZr_{0.52}Ti_{0.48}O_3$ morphotropic composition are included in italics in Table II for comparison. Differences between these monoclinic phases are also found in the octahedral tilt angles. Contrary to the *Cc* phase of $PbZr_{0.52}Ti_{0.48}O_3$, for which ω_a (ω_b) was found to be smaller than ω_c, the present monoclinic model leads to ω_a tilt angle higher than ω_c (see Fig. 10). As expected, tilt angles are found to decrease to zero when the F_{LT}-F_{HT} phase transition occurs. Following the observed behavior of the superlattice reflections, strong dependence on the thermal history of the sample is observed for the tilt angles. This can be easily understood considering that the superlattice reflections are essentially due to oxygen displacements.

E. Low-symmetry phases

This study unambiguously shows that the symmetry of the low and the high temperature ferroelectric phases is lower than rhombohedral, which has been widely accepted until now. The present results are consistent with a number of recent studies on PZT solid solutions and other lead-based ferroelectric perovskites. First of all, in a neutron diffraction study on $PbZr_{0.54}Ti_{0.46}O_3$, the boundary on the zirconium-rich side of the MPB region that separates the rhombohedral from monoclinic phases was reported not to be vertical.[27] This result has been confirmed recently by first principles calculations.[15] In their Letter, the authors have reported a calculated phase diagram for which the following sequences $Pm3m \rightarrow P4mm \rightarrow Cm \rightarrow R3m \rightarrow R3c$ and $Pm3m \rightarrow P4mm \rightarrow Cm \rightarrow Cc \rightarrow R3c$ are predicted, on decreasing temperature, for x_{Ti}=47.2% and x_{Ti}=47.5%, respectively. It is quite surprising that on decreasing temperature, the solid solution adopts lower symmetry configurations and then reverts to a higher symmetry structure (namely, *R*3*m* or *R*3*c*). The presence of monoclinic *Cm* and *Cc* structures instead of the rhombohedral phases would give much more consistent sequences. Moreover, electron diffraction patterns of rhombohedral PZT exhibit superlattice reflections of $\frac{1}{2}(hkl)_{pc}$, where $h=k=l$ (termed R_1 reflections).[38] It should be noted that these superlattice reflections are forbidden in rhombohedral symmetry. A triclinic *P*1 model was proposed to account for the observation of these reflections,[38] as a reduction in symmetry gives rise to more superlattice reflections. Simulated electron diffraction patterns did exhibit these R_1 reflections, but as they were too weak with respect to those experimentally observed, it was concluded that octahedral tilts and distortions alone are insufficient to give rise to such intense

superlattice reflections. Therefore, a further model with local regions presenting antiparallel cation displacements was proposed. In our neutron diffraction profiles of the tilted phase, there are no trace of superlattice $\frac{1}{2}(hkl)_{pc}$ reflections with $h=k=l$. However, it has been reported for the Cc phase[12] that the $\frac{1}{2}(hhh)$ reflections were observed by electron diffraction experiments but not by neutron diffraction because of their much lower structure factors with respect to those of the $\frac{1}{2}(hkl)$ reflections. From a microstructural point of view, the presence of rhombohedral symmetry is also questionable. Transmission electron microscopy studies of "rhombohedral" PZT[39,40] have shown that the ferroelectric domain configuration is more complicated than the herringbonelike configuration that is expected for rhombohedral symmetry. Wedge-shaped domains resulting from misoriented ferroelectric domain walls (which do not correspond to crystallographic planes) are, in fact, the most commonly observed configuration for these compositions and are probably a sign of a lower symmetry. The change in polarization direction between the equivalent $\langle 112\rangle$ directions may explain this complex domain structure. In a very recent study of the ferroelectric domain structures around the MPB, Asada and Koyama[41] reported the existence of a banded domain structure, in the Zr-rich side of the MPB, which can be identified as a phase having triclinic symmetry.

The stability field of the rhombohedral phase of $PbTiO_3$-based alloys such as $(1-x)[PbMg_{1/3}Nb_{2/3}O_3] - xPbTiO_3$ (PMN$-x$PT), $(1-x)[PbZn_{1/3}Nb_{2/3}O_3] - xPbTiO_3$ (PZN$-x$PT) $(1-x)[PbSc_{1/2}Nb_{1/2}O_3] - xPbTiO_3$ (PSN$-x$PT), and $(1-x)[PbFe_{1/2}Nb_{1/2}O_3] - xPbTiO_3$ (PFN$-x$PT) has also been reconsidered in recent studies. Evidence of a monoclinic M_B phase in addition to the monoclinic M_C phase has been reported for PMN$-x$PT[42] and PSN$-x$PT[43] solid solutions, for compositions which were believed to be rhombohedral. Furthermore, the discovery of a cubic phase, termed "X phase" because of its unresolved structure, for low PMN or PZN content in PMN$-x$PT and PZN$-x$PT solid solutions has considerably reduced the stability field of the rhombohedral $R3m$ phase.[44–46] In the case of PFN$-x$PT, the existence of a rhombohedral phase lying from pure PFN to the MPB has been totally ruled out in favor of a monoclinic M_A phase.[47]

IV. CONCLUSIONS

Variable temperature neutron diffraction data for $PbZr_{0.6}Ti_{0.4}O_3$ were refined by the Rietveld refinement method with a large number of structural models, namely, single- and two-phase models of rhombohedral, monoclinic, and triclinic symmetries. We have shown that structural models with a monoclinic symmetry yield significantly better agreement factors than their rhombohedral counterparts and that the spontaneous polarization lies close to the [112] pseudocubic direction instead of along the [111] direction. These low-symmetry phases appear to be a general feature for a wide range of PZT compositions over significant ranges of pressure and temperature and have major implications for the domain structure of these materials.

ACKNOWLEDGMENTS

We would like to gratefully acknowledge Jean-Louis Sauvajol (LCVN, Montpellier) for the use of the Raman spectrometer, Laurent Chapon (ISIS UK) for assistance with the experiment on GEM, and Alexandre Alapetite (IT University of Copenhagen, DK) for his advice on the writing style.

*Author to whom correspondence should be addressed. gfraysse@lpmc.univ-montp2.fr

[1] B. Jaffe, W. R. Cook, and H. Jaffe, *Piezoelectric Ceramics* (Academic, London, 1971).
[2] A. Amin, R. E. Newham, L. E. Cross, and D. E. Cox, J. Solid State Chem. **37**, 248 (1981).
[3] B. Noheda, D. E. Cox, G. Shirane, R. Guo, B. Jones, and L. E. Cross, Phys. Rev. B **63**, 014103 (2000).
[4] S. K. Mishra, D. Pandey, and A. P. Singh, Appl. Phys. Lett. **69**, 1707 (1996).
[5] B. Noheda, D. E. Cox, G. Shirane, J. A. Gonzalo, L. E. Cross, and S.-E. Park, Appl. Phys. Lett. **74**, 2059 (1999).
[6] R. Guo, L. E. Cross, S.-E. Park, B. Noheda, D. E. Cox, and G. Shirane, Phys. Rev. Lett. **84**, 5423 (2000).
[7] H. Fu and R. E. Cohen, Nature (London) **403**, 281 (2000).
[8] Ragini, S. K. Mishra, D. Pandey, H. Lemmens, and G. Van Tendeloo, Phys. Rev. B **64**, 054101 (2001).
[9] R. Ranjan, Ragini, S. K. Mishra, D. Pandey, and B. J. Kennedy, Phys. Rev. B **65**, 060102(R) (2002).
[10] D. M. Hatch, H. T. Stokes, R. Ranjan, Ragini, S. K. Mishra, D. Pandey, and B. J. Kennedy, Phys. Rev. B **65**, 212101 (2002).
[11] J. Frantti, S. Ivanov, S. Eriksson, H. Rundlöf, V. Lantto, J. Lappalainen, and M. Kakihana, Phys. Rev. B **66**, 064108 (2002).
[12] B. Noheda, L. Wu, and Y. Zhu, Phys. Rev. B **66**, 060103(R) (2002).
[13] D. E. Cox, B. Noheda, and G. Shirane, Phys. Rev. B **71**, 134110 (2005).
[14] Rajeev Ranjan, Akhilesh Kumar Singh, Ragini, and Dhananjai Pandey, Phys. Rev. B **71**, 092101 (2005).
[15] I. A. Kornev, L. Bellaiche, P.-E. Janolin, B. Dkhil, and E. Suard, Phys. Rev. Lett. **97**, 157601 (2006).
[16] D. I. Woodward, J. Knudsen, and I. M. Reaney, Phys. Rev. B **72**, 104110 (2005).
[17] J. Knudsen, D. I. Woodward, and I. M. Reaney, J. Mater. Res. **18**, 262 (2003).
[18] D. L. Corker, A. M. Glazer, R. W. Whatmore, A. Stallard, and F. J. Fauth, J. Phys.: Condens. Matter **10**, 6251 (1998).
[19] A. M. Glazer, P. A. Thomas, K. Z. Baba-Kishi, G. K. H. Pang, and C. W. Tai, Phys. Rev. B **70**, 184123 (2004).
[20] Ragini, R. Ranjan, S. K. Mishra, and D. Pandey, J. Appl. Phys. **92**, 3266 (2002).
[21] D. Pandey and Ragini, Z. Kristallogr. **218**, 1 (2003).
[22] H. Liu, R. Harrison, and A. Putnis, J. Appl. Phys. **90**, 6321 (2001).

[23] J. Rouquette, J. Haines, V. Bornand, M. Pintard, Ph. Papet, R. Astier, J. M. Léger, and F. Gorelli, Phys. Rev. B **65**, 214102 (2002).
[24] J. Rouquette, J. Haines, V. Bornand, M. Pintard, Ph. Papet, W. G. Marshall, and S. Hull, Phys. Rev. B **71**, 024112 (2005).
[25] A. C. Larson and R. B. Von Dreele, *GSAS: General Structure Analysis System* (Los Alamos National Laboratory, Los Alamos, NM, 1994).
[26] P. W. Stephens, J. Appl. Crystallogr. **32**, 281 (1999).
[27] J. Frantti, S. Eriksson, S. Hull, V. Lantto, H. Rundlöf, and M. Kakihana, J. Phys.: Condens. Matter **15**, 6031 (2003).
[28] J. Frantti, S. Eriksson, S. Hull, S. Ivanov, V. Lantto, J. Lappalainen, and K. Kakihana, J. Eur. Ceram. Soc. **24**, 1141 (2004).
[29] J. Rouquette, J. Haines, V. Bornand, M. Pintard, Ph. Papet, and J. L. Sauvajol, Phys. Rev. B **73**, 224118 (2006).
[30] J. Rouquette, J. Haines, V. Bornand, M. Pintard, Ph. Papet, B. Bonnet, and F. A. Gorelli, Solid State Sci. **5**, 451 (2003).
[31] K. A. Schönau, L. A. Schmitt, M. Knapp, H. Fuess, Rudiger-A. Eichel, H. Kungl, and M. J. Hoffmann, Phys. Rev. B **75**, 184117 (2007).
[32] A. M. Glazer, Acta Crystallogr., Sect. A: Cryst. Phys., Diffr., Theor. Gen. Crystallogr. **31**, 756 (1975).
[33] A. M. Glazer, Acta Crystallogr., Sect. B: Struct. Crystallogr. Cryst. Chem. **28**, 3384 (1972).
[34] R. Eitel and C. A. Randall, Phys. Rev. B **75**, 094106 (2007).
[35] K. C. V. Lima, A. G. Souza Filho, A. P. Ayala, J. Mendes Filho, P. T. C. Freire, F. E. A. Melo, E. B. Araujo, and J. A. Eiras, Phys. Rev. B **63**, 184105 (2001).
[36] A. G. Souza Filho, K. C. V. Lima, A. P. Ayala, I. Guedes, P. T. C. Freire, F. E. A. Melo, J. Mendes Filho, E. B. Araujo, and J. E. Eiras, Phys. Rev. B **66**, 132107 (2002).
[37] J. Rouquette, J. Haines, V. Bornand, M. Pintard, Ph. Papet, and F. A. Gorelli, J. Eur. Ceram. Soc. **25**, 2093 (2005).
[38] J. Ricote, D. L. Corker, R. W. Whatmore, S. A. Impey, A. M. Glazer, J. Dec, and K. Roleder, J. Phys.: Condens. Matter **10**, 1767 (1998).
[39] J. Ricote, R. W. Whatmore, and D. J. Barber, J. Phys.: Condens. Matter **12**, 323 (2000).
[40] L. A. Schmitt, K. A. Schönau, R. Theissmann, H. Fuess, H. Kungl, and M. J. Hoffmann, J. Appl. Phys. **101**, 074107 (2007).
[41] T. Asada and Y. Koyama, Phys. Rev. B **75**, 214111 (2007).
[42] A. K. Singh, D. Pandey, and O. Zaharko, Phys. Rev. B **74**, 024101 (2006).
[43] R. Haumont, A. Al-Barakaty, B. Dkhil, J. M. Kiat, and L. Bellaiche, Phys. Rev. B **71**, 104106 (2005).
[44] G. Xu, D. Viehland, J. F. Li, P. M. Gehring, and G. Shirane, Phys. Rev. B **68**, 212410 (2003).
[45] G. Xu, H. Hiraka, G. Shirane, and K. Ohwada, Appl. Phys. Lett. **84**, 3975 (2004).
[46] M. Gehring, W. Chen, Z.-G. Ye, and G. Shirane, J. Phys.: Condens. Matter **16**, 7113 (2004).
[47] S. P. Singh, A. K. Singh, and D. Pandey, J. Phys.: Condens. Matter **19**, 036127 (2007).
[48] C. M. Foster, Z. Li, M. Grimsditch, S.-K. Chan, and D. J. Lam, Phys. Rev. B **48**, 10160 (1993).
[49] J. Rouquette, J. Haines, G. Fraysse, V. Bornand, M. Pintard, Ph. Papet, and F. A. Gorelli (unpublished).